JOURNAL OF MATERIALS SCIENCE 18 (1983) 732–740

Microstructural aspects of impact erosion in single crystals of LiF, NaCl, KCl and CaF_2 by blunt projectiles

SUSAN R. SCHUON*, K. N. SUBRAMANIAN
Department of Metallurgy, Mechanics and Materials Science, Michigan State University, East Lansing, Michigan 48824, USA

In an attempt to clarify the fundamental mechanism of material removal in erosion by blunt solid particles entrained in a fluid stream impinging on a solid surface, single crystals of CaF_2 (relatively brittle), LiF (intermediate between brittle and ductile), and KCl and NaCl (relatively ductile) were eroded with 0.25 mm glass beads and 0.50 mm quartz sand grains. The velocity of the particles was varied between 2 and 120 m sec^{-1}. Erosion damage was studied with optical and scanning electron microscopy. In the single-impact mode, the damage is highly dependent on the mechanical properties of the target; material spalled off or micromachined out in individual impacts, or as chips produced upon the intersection of fractures resulting from several neighbouring impacts. At normal impact, the predominant mechanism is intersecting fractures, but at impact angles away from the normal, micromachining occurs in NaCl and KCl and, in fact, becomes the major mechanism of material removal. In LiF, only a little micromachining occurs and in CaF_2, none at all; hence in these materials spalling is the controlling mechanism for material loss in individual impacts.

1. Introduction

To gain a better understanding of the fundamental mechanism of erosion, single crystals of LiF, NaCl, KCl and CaF_2 are ideal models because they have simple, well-known crystal structures and slip systems [1–8]. The first three have rock-salt structure and the last one has fluorite structure.

Many investigators have observed distinct periods of erosion, such as incubation, acceleration, deceleration and steady-state periods [9–15]. Microstructural studies in ductile materials show that massive plastic flow occurs during the incubation period [16, 17]. In brittle materials, Hoff *et al.* [18] observed a critical velocity below which there is no erosion and above which ceramics and glasses fail rapidly owing to severe crack propagation. Metals, which erode at lower velocities, are more resistant above the critical velocity, as they can still deform before complete destruction. Notch-impact strength has been suggested as a criterion for erosion reistance of brittle materials [18, 19]. In oblique impact, micromachining has been proposed as a major mechanism of metal removal [20–23]. During impact, material flows uniformly outward from the front and sides of the particles until the displaced material is strain-hardened enough to fracture [20].

Wiederhorn and Roberts [24], in studying the mode of erosion of a castable refractory, observed that at 25° C material loss occurred by brittle fracture, and that at temperatures above 1000° C material loss occurred by shear deformation. Hockey *et al.* [19], and Sheldon [23] have also found a dependence of the extent and mode of erosion on the angle of impact.

Most theories of erosion of brittle materials are based on Hertz's analysis of the stresses generated when an isotropic elastic sphere is pressed quasistatically against a flat, isotropic half space [25, 26]. Physical damage arises from a charac-

*Present address: NASA-Lewis, Cleveland, Ohio 44135, USA.

 0022–2461/83/030732–09$03.58/0

teristic Hertzian cone crack [27]. This crack is proposed to develop from a random flaw situated in the superficial region of high stress near the circle of contact. The crack, which has the shape of the frustum of a cone, penetrates the solid by a distance determined by the magnitude of the load. Two or more cracks must intersect for material loss to occur. Finnie [28] combined Hertz's analysis with Weibull's statistical treatment of the effect of flaws and shows that brittle materials start to erode in a characteristically ductile manner if the erosive particles are sufficiently small, since the probability of a critical size flaw decreases as the particle size decreases. Lawn and Wilshaw [27] observed that impact damage under fully plastic contact conditions is identical in form to that obtained under quasi-static conditions producing radial, lateral and median cracks outside a central plastic impression. The appearance of damage suggests that Lawn's [27, 29–35] theories of deformation under blunt indenters may be applicable to the erosion behaviour of brittle materials. According to Lawn, for blunt indenters in perfectly elastic contact, crack initiation is controlled by pre-existing flaws at the specimen surface; fracture begins from a pre-existing flaw and grows by running horizontally around the contact in a radial stress field, closely following circular stress trajectories. Lawn and Wilshaw [27] also suggest that there is some compromise between the tendency for cracks in single crystals to follow stress trajectories and cleavage planes. Adler [36] studied the impact-erosion behaviour of silicate glass impacted by blunt projectiles (glass beads), and found that the major mode of damage was through the formation of a Hertzian cone fracture, and that the material loss occurred when the lateral fractures intersected.

The objective of this work is to determine the role of microscopic deformation on macroscopic erosion damage. Another objective of this study is to determine the relationship between material properties and the critical velocity required to produce erosion damage. Ultimately, an objective of this study is to understand the basic mechanisms of deformation of brittle and semi-brittle crystals under dynamic loading.

2. Experimental procedure

Test samples of single crystals (approximately 10 mm × 5 mm × 3 mm) were obtained by cleaving from bulk crystals. Glass beads and standard Ottowa quartz sand were used as blunt projectiles to produce erosion damage. Glass beads had a bimodal distribution in diameter: 95% had an average diameter of 0.25 mm with standard deviation of 0.035 mm, and the rest had an average diameter of 0.05 mm with a standard deviation of 0.01 mm. Weathered and rounded sand had an average diameter of 0.50 mm with a standard deviation of 0.02 mm. Both these projectiles have a hardness of approximately 7 on the Mohs' scale.

Samples were eroded with particles accelerated by nitrogen carrier gas. Particle velocity was determined by a method developed by Ruff and Ives [37]. Exposure time, which was usually few seconds, was controlled with a rotating disc (which had a 20° wedge cut out of it) by controlling its angular velocity. The samples were held on an aluminium rod, whose orientation can be changed at a distance of 2 cm below the exit end of the nozzle. Approximately 50 mm^2 area of the sample was exposed to erosion. Elevated temperature testing was also carried out with samples of LiF at 200 and 400° C inside a furnace. To avoid thermal stresses in the sample during testing, the carrier gas was preheated to the test temperature by passing it through a copper tube placed within the furnace.

After testing, specimens were examined by optical and scanning electron microscopy. Eroded surfaces of LiF and CaF_2 samples were etched and studied to understand the role of plastic deformation in erosion damage.

3. Results and discussion

Damage produced by single impact is analysed in Sections 3.1 to 3.4; multiple impact, where impacts are sufficiently close for their effects to interact, is considered in Section 3.5.

3.1. Normal impact of projectiles at room temperature

The critical velocity is defined as the velocity of impact at which lateral fractures appear in ceramic materials. These lateral cracks which radiate outwards from the point of impact can be seen in Fig 1a. The critical velocity is much lower in CaF_2 than in more ductile materials such as LiF, NaCl and KCl. In CaF_2 lateral fractures develop at velocities of less than 2 $m\,sec^{-1}$ as shown in Fig. 1a. As the ductility of the material increases, the critical velocity increases. At impact velocities below critical, only microslip occurs at the area of

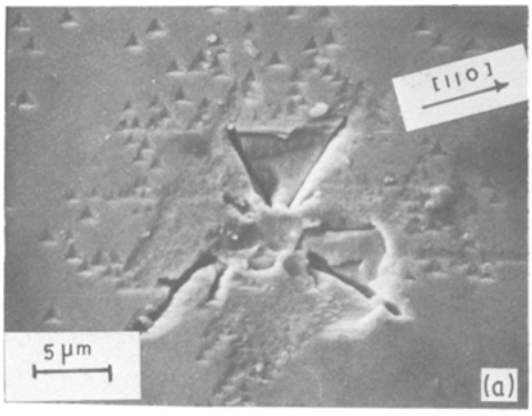

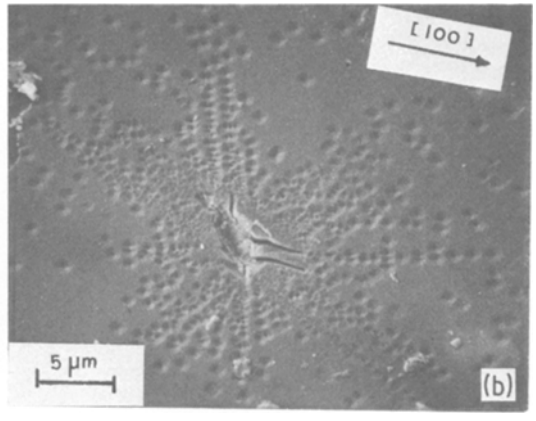

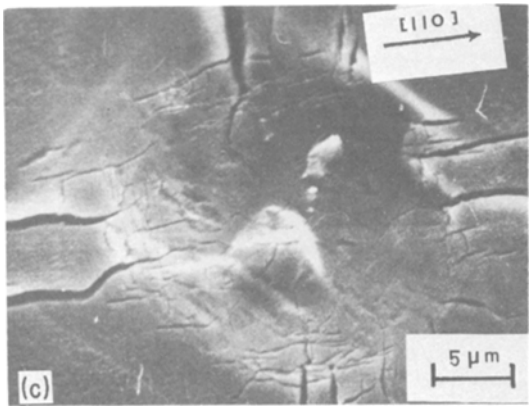

Figure 1 Scanning electron micrographs of crystals eroded by normal impact of projectiles by 0.25 mm glass beads. (a) CaF_2 eroded on {111} at a velocity of 2 m sec^{-1}, (b) LiF eroded on {100} at a velocity of 10 m sec^{-1}, (c) LiF erored on {100} at a velocity of 45 m sec^{-1}. Microfractures which appear to be curved can be ssen in this figure. Lateral cracks radiating from the point of impact can be seen in (a) and (c).)

impact, evidence for which is the rosette pattern of dislocation etch-pits formed along the {1 1 0} slip plane traces in Fig. 1b. Even in CaF_2, slip occurs at low impact velocities in the {1 0 0} ⟨0 1 1⟩ slip system, as can be observed in Fig. 1a. The contact zone for a blunt indenter is characterized by massive plastic flow, and microfractures within the region of contact is extensive, as shown in Fig. 1c. These microfractures, which appear curved depart from specific crystallographic directions.

Stress fields might have caused non-cleavage fracture to account for this observation as predicted by Lawn and Wilshaw [27]. However, these curved microfractures may be due to reorientation of crystal segments cleaved during impact and reoriented to produce an appearance of curved boundaries. In the case of ductile crystals, such as KCl and NaCl, plastic flow is extensive. At impact velocities greater than 25 m sec^{-1}, embedding of whole projectiles can occur in KCl, as shown in Fig. 2. In LiF (intermediate ductility), embedding of whole projectiles is never observed although at impact velocities greater than 30 m sec^{-1}, some fragmentation and embedding of projectile fragments has been found by microprobe examination. In brittle CaF_2, embedding of neither projectiles nor projectile fragments is observed.

Unlike more ductile materials, CaF_2 does not exhibit extensive plastic deformation in the contact zone. Extensive microfracturing, however, does occur, as seen in Fig. 3a. Often a complete ring fracture is developed at the zone perimeter, and lateral fractures are developed outside the contact zone. In NaCl-structured crystals,

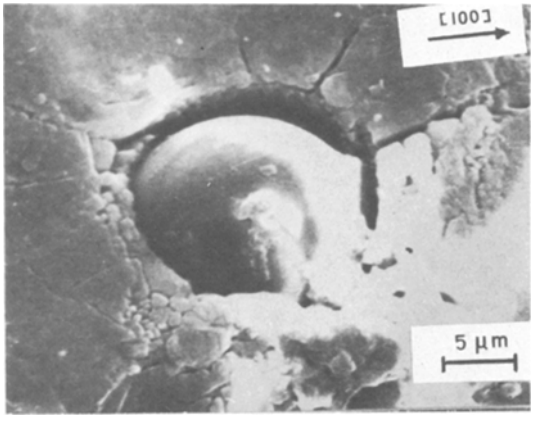

Figure 2 Scanning electron micrograph of KCl eroded by 0.25 mm glass beads impacting the {0 0 1} at a velocity of 25 m sec^{-1}. (Impacted bead is much smaller than the average size of the beads used as projectiles.)

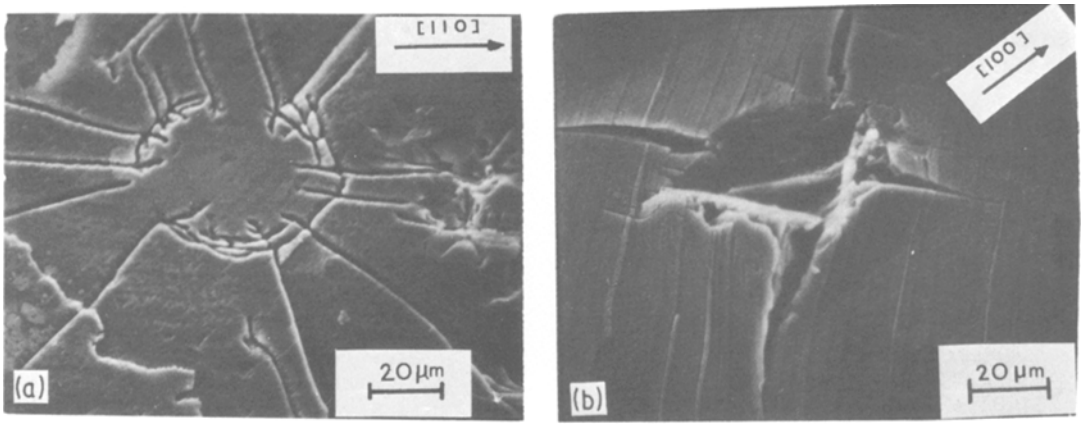

Figure 3 Microfractures produced during normal impact. (a) CaF_2 eroded by impacting 0.25 mm glass beads on {1 1 1} at a velocity of 30 m sec^{-1}. (b) LiF eroded by 0.5 mm sand particles on {1 0 0} at a velocity of 45 m sec^{-1}.

which are less brittle, four lateral fractures result during normal impact as illustrated in Fig. 3b. These fractures originate outside the contact zone. Although numerous microfractures occur just within the circle of contact, usually only four major lateral fractures are developed outside it. A ring fracture is usually not fully developed unlike in the case of silicate glasses [36].

In NaCl and KCl, fractures are developed as a result of dislocation reaction:

$$(a/2)\,[0\,1\,1]_{(01\bar{1})} + (a/2)\,[0\,1\,\bar{1}]_{(011)} \rightarrow a\,[0\,1\,0]_{(010)},$$

producing fracture on the (0 1 0). In LiF, lateral fractures are formed through the reaction:

$$(a/2)\,[1\,0\,\bar{1}]_{(101)} + (a/2)\,[0\,\bar{1}\,1]_{(011)} \rightarrow (a/2)\,[1\,\bar{1}\,0]_{(112)}.$$

The reacted $(a/2)\,[1\,\bar{1}\,0]$ edge dislocation has a line vector parallel to the $(a/3)\,[1\,1\,\bar{1}]$. This dislocation is contained in the (1 1 2), and is sessile for NaCl-structured crystals. Once the dislocations have reacted they prevent additional displacement of the crystal along the [0 0 1]. This downward displacement is necessary to maintain negligible volume change for the continuing impact process [38]. Cleavage along the [1 1 0] allows for upward displacement of the crystal. A crater produced by {1 1 0} cleavage will be pyramidal with four flat faces. Superficially, this fracture pattern mimics a classic Hertzian cone fracture as shown in Fig. 4. The crater surface predominantly consists of {1 1 0} cleavage planes. However, deviation of crater surface from cleavage plane to make it more conical by non-cleavage fracture can be observed in this micrograph.

In CaF_2, fracture due to particle impact occurs along {1 0 0}, {1 1 0}, and {1 1 1}. Of these {1 1 1} are primary cleavage planes. The dislocation reaction causing {1 0 0} and {1 1 0} fractures can be represented by

$$\tfrac{1}{2}\,a\,[0\,\bar{1}\,1] + \tfrac{1}{2}\,a\,[0\,\bar{1}\,\bar{1}] = a[0\,\bar{1}\,0],$$

and

$$\tfrac{1}{2}\,a\,[0\,\bar{1}\,\bar{1}] + \tfrac{1}{2}\,a\,[1\,0\,1] = \tfrac{1}{2}\,a\,[1\,\bar{1}\,0],$$

respectively. Although {1 1 1} is the primary cleavage plane, a crack formed on a {1 1 1} face must pass through dislocation pile-ups at {1 0 0} intersections [39]. These regions are regions of high stress that oppose the tensile stress aiding the propagation of the crack. As a result, {1 0 0} fractures were found to be more common than

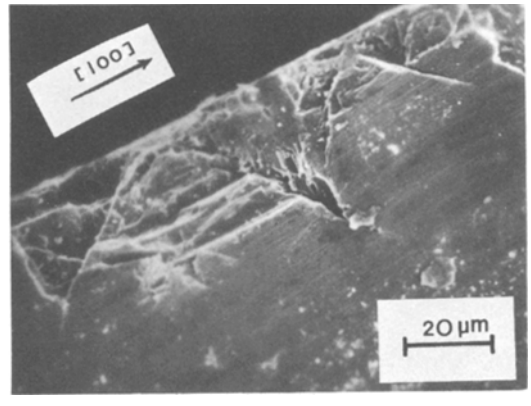

Figure 4 Fracture in LiF eroded by 0.25 mm glass beads impacting the (0 0 1) at a velocity of 45 m sec^{-1}. The plane of observation is (0 1 0).

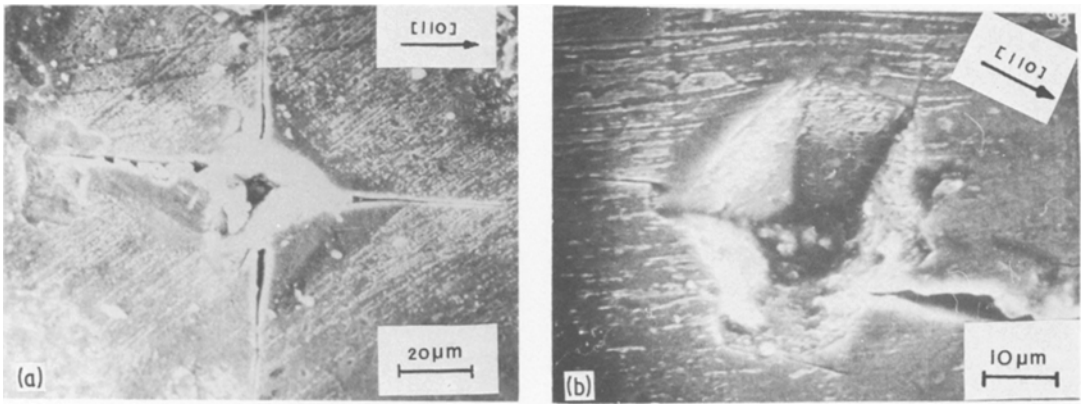

Figure 5 LiF impacted by 0.5 mm sand particles on {100} plane with a projectile velocity of 45 m sec^{-1} (a) at 200° C, (b) 400° C.

{110} fractures. These cracks propagate more readily along the surface, but encounter difficulty in propagating into the interior of the crystal, resulting in chips characteristically much shallower than the length of the fracture. The high stress field around the zone of contact, and the difficulty of {100} and {110} fractures in propagating into the interior of the crystal lead to the formation of conchoidal fracture similar to those observed by Phillips [7] in CaF_2 and by Evans [31] in ZnS.

3.2. Normal impact of projectiles at elevated temperatures

Erosion tests were carried out at 200 and 400° C on the cleavage plane of LiF crystals. At these temperatures, a secondary slip system {100} ⟨011⟩ also becomes active and, as a result, deformation can be accommodated more easily. Within the contact zone, microfracturing, prominent at lower temperature, is absent and instead a faceted appearance develops due to impacts at these temperatures as shown in Fig. 5. Lateral fractures are not observed in specimens eroded at 400° C. At an angle of impact of 30° from normal, at 200° C, only two lateral fractures are present on one side, although room-temperature tests exhibit two longer and two shorter lateral cracks on opposite sides of the contact zone. An overall increase in plasticity with increasing temperature leads to a decrease in brittle failure during impact in LiF.

3.3. Oblique impact of projectiles at room temperature

Micromachining becomes an important mode of erosion at angles of impact greater than 30° from the normal in LiF, NaCl and KCl. The surface damage in KCl eroded at an angle of 60° from the normal, as shown in Fig. 6a is a furrow formed as the particles grazes and travels across the surface pushing the material ahead of it to the side. No large longitudinal fractures outside the line of contact occur. However, microfracture, as illustrated in Fig. 6b, occurs along the furrow in {100} planes as a consequence of material work-hardening and resultant fracture. Micromachining occurs at velocities as low as 2 m sec^{-1}.

The degree of micromachining by oblique impact in LiF is less extensive than in NaCl and KCl. Although a limited amount of micromaching occurs in LiF at angles of impact 60° from normal, the major mode of damage is through the development of lateral fractures. The number and length of these fractures are affected by the angle of impact. At an angle of impact of 30° from the normal, as shown in Fig. 6c, four lateral fractures are developed, but they are no longer of equal length. Only two lateral fractures are developed outside the circle of contact, as shown in Fig. 6d, when the angle of impact is 60° from the normal, as a consequence of highly asymmetrical distribution of applied stress.

CaF_2 exhibits no micromachining during oblique impact, as shown in Fig. 6e. Although limited slip is observed, damage occurs by the development of lateral fractures. The length of these lateral fractures also varies with the angle of impact in a manner similar to that observed in LiF.

3.4. The relationship of blunt projectile damage to the Hertzian stress field

Several investigators [28, 30, 31, 36] have suggested that Hertz's analysis of the stresses generated when

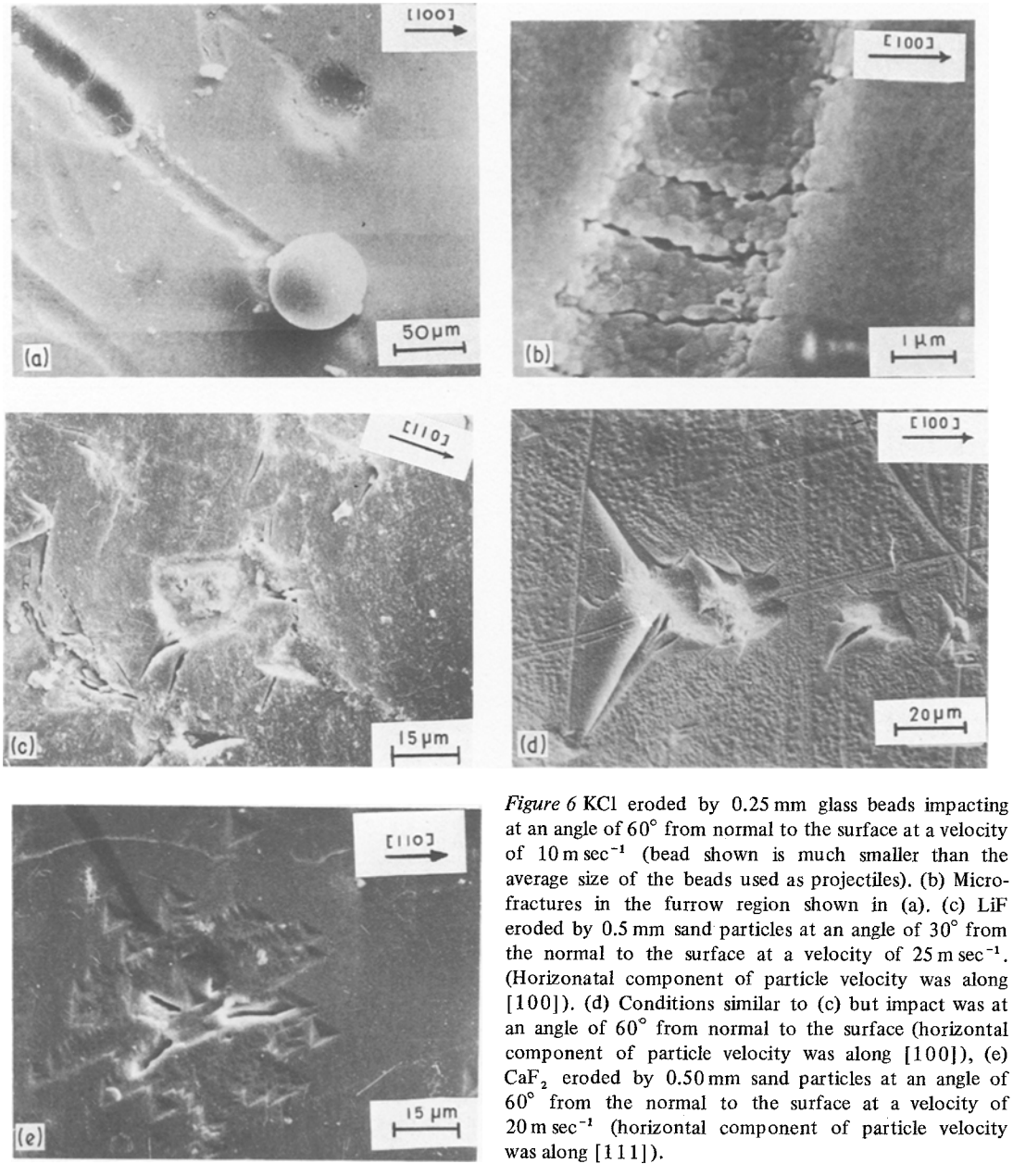

Figure 6 KCl eroded by 0.25 mm glass beads impacting at an angle of 60° from normal to the surface at a velocity of 10 m sec^{-1} (bead shown is much smaller than the average size of the beads used as projectiles). (b) Microfractures in the furrow region shown in (a). (c) LiF eroded by 0.5 mm sand particles at an angle of 30° from the normal to the surface at a velocity of 25 m sec^{-1}. (Horizonatal component of particle velocity was along [100]). (d) Conditions similar to (c) but impact was at an angle of 60° from normal to the surface (horizontal component of particle velocity was along [100]), (e) CaF_2 eroded by 0.50 mm sand particles at an angle of 60° from the normal to the surface at a velocity of 20 m sec^{-1} (horizontal component of particle velocity was along [111]).

an isotropic elastic sphere is pressed quasi-statically against a flat, isotropic half-space may help to predict the damage caused by the impact of a blunt projectile on the surface of the material. In this study, we compared the diameter of the observed contact zone with that predicted by Hertz's analysis.

At normal impact the diameter of the contact zone increases with increase in projectile velocity, as shown in Fig. 7a and b. Softer crystals such as KCl and NaCl show a greater increase in the diameter of circle of contact with increase in velocity than CaF_2 and LiF. The diameter of contact zone as a function of velocity, calculated by Hertz's analysis is presented in Fig. 7c. The observed values are larger than the calculated values by a factor of about 10 for CaF_2 and LiF, and by a factor of about 20 for KCl and NaCl. The discrepancy probably stems from the neglect of plastic deformation in the Hertz analysis.

The length of lateral fractures increases with increasing diameter of contact zone as shown in Fig. 7d.

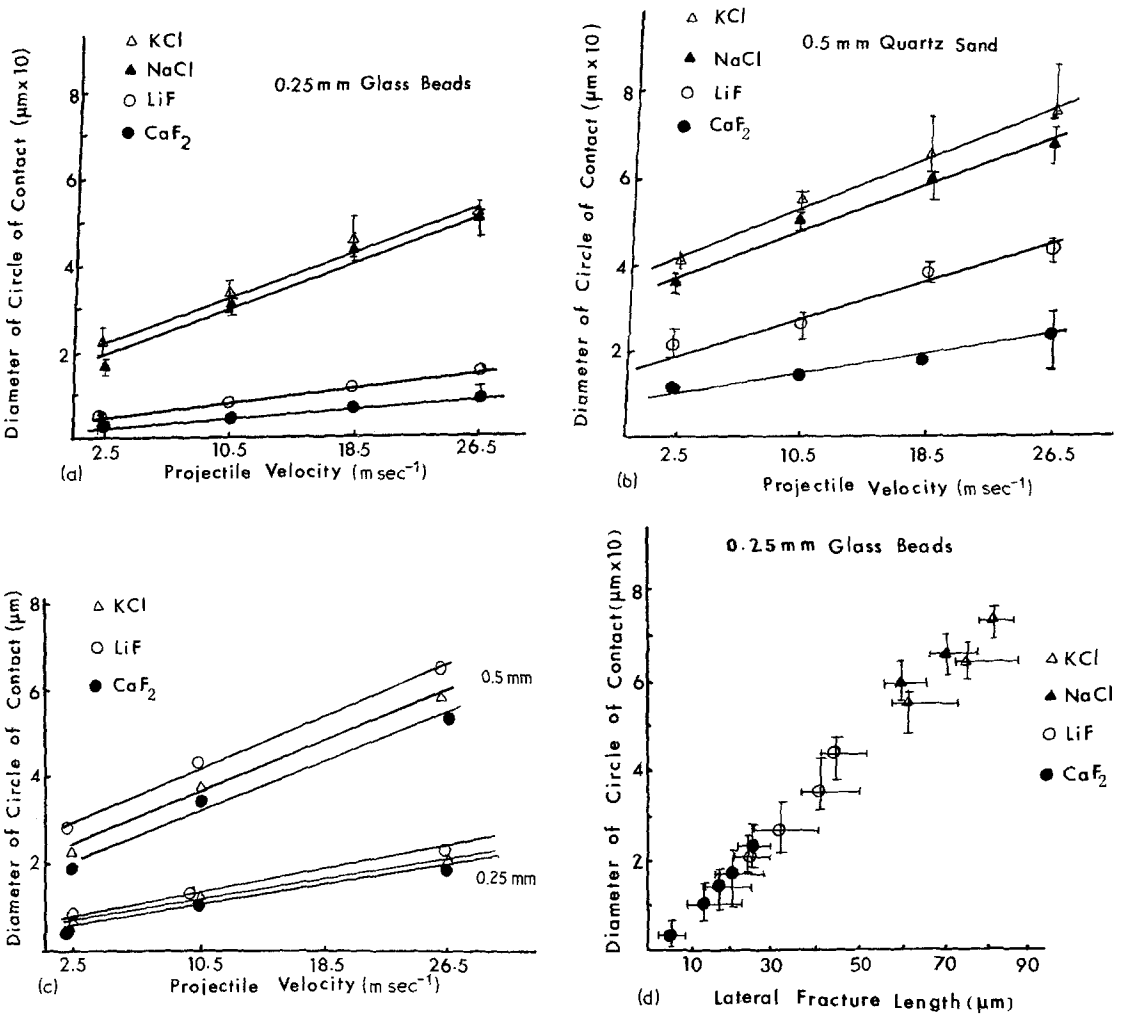

Figure 7 Plot of the diameter of the circle of contact against (a) the impact velocity of 0.25 mm glass beads, (b) the impact velocity of 0.5 mm sand particles, (c) the projectile velocity calculated using Hertz's analysis, (d) the length of lateral fractures.

3.5. Impact erosion damage produced by multiple blunt projectile at room temperature

In single-impact damage by blunt projectiles, weight loss is seldom observed. In multiple impact, on the other hand, the intersection of lateral fractures, even two single impacts in brittle material like CaF_2, produce material loss as shown in Fig. 8a. In CaF_2 the extent of plastic deformation is considerably less. In this material, material loss can occur by single impact (by forming chips) or by intersection of lateral fractures in multiple impact, although the latter is responsible for greater material removal. In LiF, on the other hand, material loss does not occur from the intersection of the lateral fractures from a pair of single impacts. In LiF extensive deformation is necessary before material loss occurs through the intersection of lateral fractures. A critical density of lateral fractures is necessary before significant material loss occurs. In KCl and NaCl substantial deformation and work-hardening occurs before significant material loss is observed.

Loss of material occurs through the intersection of fractures in a mode similar to that observed by Adler [36] for the erosion of glass by blunt projectiles. This mode appears to apply best to brittle material such as CaF_2. In ductile materials, at large particle velocities, fracture extension occurs resulting in cleavage and loss of a large volume of material as shown in Fig. 8b. As material is removed, a new, relatively undisturbed surface is exposed to further erosion. In oblique impact, micromachining becomes an important

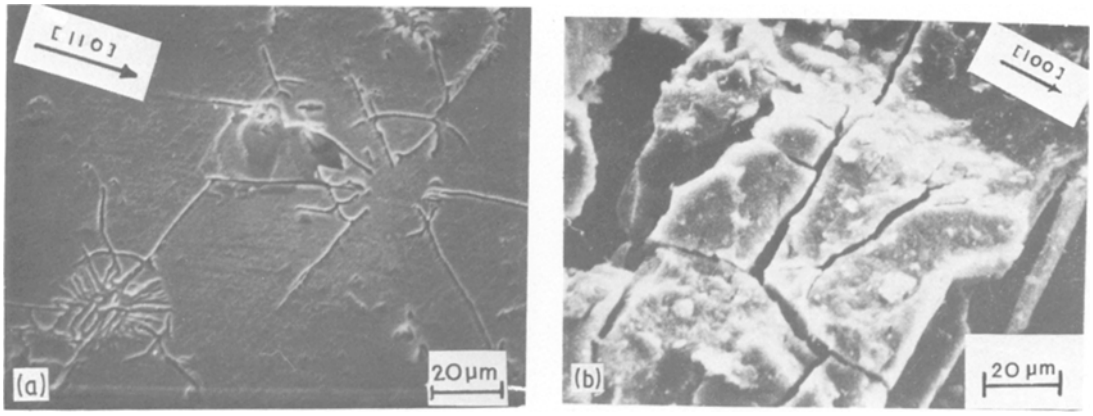

Figure 8 (a) Intersection of lateral fractures causing material loss in CaF_2 eroded by 0.25 mm glass beads at a velocity of 25 m sec^{-1}. (b) Loss of material in KCl eroded by 0.25 mm glass beads at a velocity of 75 m sec^{-1}.

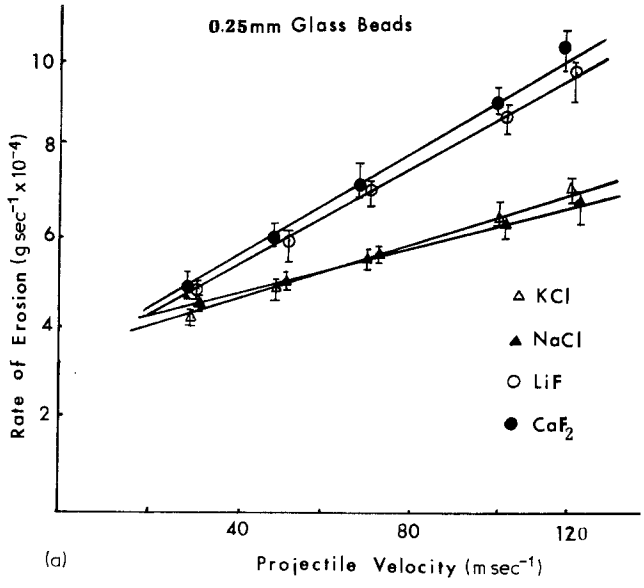

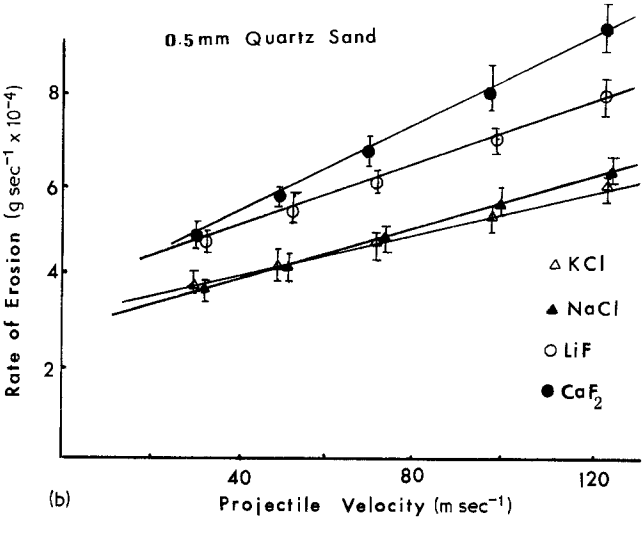

Figure 9 Rate of erosion against the impact velocity (a) with 0.25 mm glass beads, (b) with 0.5 mm sand particles.

mode of damage in soft materials and the erosion rate decreases compared to normal impact as a result of increased plastic flow.

The plasticity of the material affects the rate of erosion. NaCl and KCl have a lower rate of erosion than either CaF_2 or LiF as shown in Fig. 9. The rate of erosion increases with the projectile size possibly as the result of an increase in the length of lateral fractures with the increase in projectile diameter.

As in metals, erosion in halide single crystals is characterized by an incubation period; unlike the case in metals, a steady state period is not observed.

4. Conclusions

(1) Damage produced by a single normal impact of blunt projectile is characterized by a contact zone and a set of lateral fractures occuring outside this zone. The contact zone shows damage by extensive plastic flow and intense microfracturing. In contrast, the lateral fractures lie exclusively along specific crystallographic directions. Although the damage superficially resembles a Hertzian cone fracture, the damage differs in that lateral fractures do not follow the path predicted by the Hertzian stress field.

(2) In LiF, normally impacted on the cleavage plane at elevated temperatures (200 and 400° C), microfracturing is absent and the contact zone has a faceted appearance.

(3) The length of the lateral fractures in normal impact is proportional to the diameter of the contact zone. The diameter of the circles of contact calculated by Hertz's analysis is much smaller than the observed values.

(4) In oblique impact, micromachining, as proposed by Finnie [20] becomes an important mode of surface damage in KCl and NaCl. The importance of micromachining decreases with decreased ductility of the material, however, and in LiF and CaF_2 the intersection of lateral fractures remains as the major mode of material loss.

References

1. J. WASHBURN, "Electron Microscopy and Strength of Crystals", edited by Thomas and J. Washburn (Interscience, New York, 1963) p. 301.
2. J. J. GILMAN and W. G. JOHNSON, *J. Appl. Phys.* **27** (1962) 1018.
3. *Idem, Solid State Physics* **13** (1962) 148.
4. J. J. GILMAN, *Acta Metall.* 7 (1959) 608.
5. T. L. JOHNSTON, C. H. LI and R. J. STOKES, "Strengthening Mechanisms in Solids" (ASM, Metals Park, Ohio, 1962) p. 341.
6. J. WASHBURN, *ibid.*, p. 51.
7. W. L. PHILLIPS, Jr, *J. Amer. Ceram. Soc.* **44** (1961) 499.
8. A. R. PATEL and C. C. DESAI, *Z. Kristallogr.* **121** (1965) 55.
9. T. McGUINESS and A. THIRUVENGADAM, ASTM Spec. Tech. Publ. no. 567 (1974) p. 30.
10. A. S. SPRINGER and C. B. BAX, *ibid.* p. 106.
11. M. C. ROCHESTER and J. H. BRANTON, *ibid.*, p. 128.
12. A. F. CONN and S. L. RUDY, *ibid.*, p. 239.
13. D. E. ELLIOTT, J. B. MARRIOTT and A. SMITH, ASTM Spec. Tech. Publ. no. 474 (1979) p. 127.
14. W. D. POUCHOT, *ibid.*, (1970) p. 383.
15. P. EISENBERG, *ibid.*, p. 3.
16. F. ERDMAN-JESNITZER and H. LO, ASTM Spec. Tech. Publ. no. 568 (1974) p. 171.
17. B. VYAS and C. M. PREECE, *ibid.* p. 77.
18. G. HOFF, G. LANHEIN and H. RIEGER, ASTM Spec. Tech. Publ. no. 474 (1970) p. 42.
19. B. J. HOCKEY, S. M. WIEDERHORN and H. JOHNSTON, NBSIR 77-1396 (1977).
20. I. FINNIE, *Wear* **19** (1972) 81.
21. G. P. TILLY, *ibid.* **23** (1973) 87.
22. R. E. WINTER and I. M. HUTCHINGS, *ibid.* **25** (1977) 141.
23. G. L. SHELDON, *J. Basic Eng. Trans. ASME* **62D** (1970) 619.
24. S. M. WEIDERHORN and D. E. ROBERTS, *Amer. Ceram. Soc. Bull.* **55** (1976) 185.
25. H. HERTZ, *J. Reine Angew Math.* **92** (1882) 156.
26. L. B. GRESZEZUK, ASTM Spec. Tech. Publ. no. 568 (1975) p. 183.
27. B. R. LAWN and T. R. WILSHAW, *J. Mater. Sci.* **10** (1975) 113.
28. I. FINNIE, *Wear* **3** (1960) 87.
29. F. B. LANGITAN and B. R. LAWN, *J. Appl. Phys.* **40** (1969) 4009.
30. *Idem. ibid.*, **42** (1973) 405.
31. A. G. EVANS, *J. Amer. Ceram. Soc.* **56** (1973) 405.
32. B. R. LAWN, *J. Appl. Phys.* **39** (1968) 4828.
33. B. R. LAWN, S. M. WIEDERHORN and H. H. JOHNSON, *J. Amer. Ceram. Soc.* **98** (1975) 428.
34. S. M. WIEDERHORN and B. R. LAWN, *ibid.* **60** (1977) 451.
35. F. C. FRANK and B. R. LAWN, *Proc. Roy. Soc. London, Ser. A* **299** (1967) 291.
36. W. F. ADLER, ASTM Spec. Tech. Publ. no. 567 (1974) p. 294.
37. A. W. RUFF and L. K. IVES, *Wear* **35** (1975) 195.
38. R. W. ARMSTRONG and C. CM. WU, *J. Amer. Ceram. Soc.* **61** (1978) 102.
39. A. S. KEH, *J. Appl. Phys.* **31** (1960) 1538.

Received 22 March
and accepted 16 July 1982